

# Stimulation Electrode Materials and Electrochemical Testing Methods

Andy Hung, Ira B. Goldberg, and Jack W. Judy

**Abstract** Neuro-stimulation can be implemented using several design choices — bipolar vs. monopolar stimulation, current vs. voltage control, and active vs. passive recharge. To ensure proper function through the desired lifetime, electrodes are typically made of titanium, platinum, or iridium. The difference between the 3 metals is primarily based on their performance in reversible oxidation/reduction mechanisms, which can be illustrated using various electrochemical techniques.

In slow cyclic voltammetry analysis, a platinum electrode can reversibly consume and release  $3 \text{ mC/cm}^2$  of charge within the normal operating voltage range. However, for actual neuro-stimulation pulses, platinum can only safely inject  $0.1 \text{ mC/cm}^2$ , as estimated from an electrode-potential graph. Compared to platinum, *iridium* can inject 10 times the amount of charge for both neuro-stimulation and cyclic voltammetry. The greater capability is due to both the greater number of available oxidation states and utilization of bulk porous oxide.

In AC impedance, a titanium electrode exhibits the same double-layer capacitance per area as that of platinum. However, titanium suffers from irreversible buildup of a high-impedance oxide layer, which prevents sustained charge-injection usage. The irreversible oxidation can be observed using the pulse-clamp technique.

This chapter also introduces computer simulations, specifically capacitive computer models, as a method for visualizing the current-distribution pattern. The simulation shows uniform current distribution despite prominent electrode topologies. A dissolution study performed with gold electrodes confirms that the current distribution is uniform during normal usage, but exhibits severe current crowding when charge injection is increased above the safe limit.

## Contents

|                                 |     |
|---------------------------------|-----|
| 1 Introduction . . . . .        | 192 |
| 2 Electrode Reactions . . . . . | 193 |

---

A. Hung (✉)  
Boston Scientific Neuromodulation Corporation, Valencia, CA, USA  
e-mail: andy.hung@bsci.com

|     |  |     |
|-----|--|-----|
| 2.1 | Electrode Interface . . . . .  | 193 |
| 2.2 | Electrical Double Layer . . . . .                                    | 194 |
| 2.3 | Reversible Metal Oxidation/Reduction . . . . .                       | 194 |
| 2.4 | Irreversible Chemical Reaction . . . . .                             | 195 |
| 2.5 | Electrolyte Resistance . . . . .                                     | 196 |
| 3   | Common Electrochemical Tests and Electrode Materials . . . . .       | 196 |
| 3.1 | Cyclic Voltammetry . . . . .   | 196 |
| 3.2 | Platinum . . . . .   | 198 |
| 3.3 | Titanium . . . . .   | 199 |
| 3.4 | Iridium . . . . .  | 199 |
| 3.5 | Effect of Protein . . . . .  | 201 |
| 3.6 | Impedance Measurement . . . . .                                      | 201 |
| 4   | Neural Stimulation Settings Which Affect Charge Injections . . . . . | 202 |
| 4.1 | Basis of Neural Stimulation . . . . .                                | 202 |
| 4.2 | Components of a Neural Stimulation System . . . . .                  | 203 |
| 4.3 | Monophasic Voltage Stimulation . . . . .                             | 203 |
| 4.4 | Constant Voltage vs. Constant Current . . . . .                      | 203 |
| 4.5 | Analysis of Constant-Current Electrode-Voltage Waveform . . . . .    | 204 |
| 4.6 | Current Control with Passive Recharge . . . . .                      | 205 |
| 4.7 | Active Recharge . . . . .  | 206 |
| 4.8 | Cathodic Bias . . . . .  | 207 |
| 4.9 | Bipolar vs. Monopolar Stimulation . . . . .                          | 207 |
| 5   | Other Measurement Techniques . . . . .                               | 207 |
| 5.1 | Electrode-Potential Measurement . . . . .                            | 208 |
| 5.2 | Pulse Clamp . . . . .  | 209 |
| 5.3 | Computer Simulation . . . . .  | 210 |
| 5.4 | Dissolution Testing . . . . .  | 213 |
| 5.5 | Inductively Coupled Plasma (ICP) . . . . .                           | 214 |
| 6   | Summary . . . . .  | 214 |
|     | References . . . . .   | 214 |

## 1 Introduction

Within a neural stimulation system, the electrodes are subjected to a harsh working environment. They may have to inject a large amount of charge, tolerate extreme local pH changes, and function for the duration of the device lifetime. To ensure longevity, the electrodes need to be thoroughly tested.

Traditionally, engineers prefer capacitive electrodes [1]. These electrodes are made from inert materials that do not react with surrounding electrolyte and therefore avoid corrosion. Examples of these are carbon electrodes for skin patches and titanium or tantalum electrodes for pacemakers. Since the electrodes do not employ oxidation reactions, they are limited in their charge-injection capability. Device designers try to compensate for this shortcoming by using larger electrodes and making the materials more porous to enhance the surface area.

In recent years, there has been a growing interest in applications that target neural tissues insulated by a thick dura layer, such as in spinal cord and retina. The large amount of charge injection that is required for these applications can only be safely provided by platinum and iridium electrodes. These two materials have substantial charge storage capacity within the water window (the voltage range over which water electrolysis does not occur), thereby allowing for a much higher charge-injection capability.

Titanium, platinum, and iridium materials have been shown to be well tolerated by the tissue without concerns related to toxicity. Platinum is a widely used material because of its durability and its relative ease of manufacture. Although iridium can inject even higher amounts of charge than platinum, its high mechanical strength leads to difficulties in machining or molding. Instead, it is usually sputtered or electroplated onto the electrode surface, adding complexity to the manufacturing process. Titanium is often used as a casing for the electronics, but suffers from relatively poor charge-injection capability. In this chapter, the electrochemical properties of these three materials are illustrated using various testing methods.

## 2 Electrode Reactions

### 2.1 Electrode Interface

Neural stimulation devices depend on the ability to excite the neural cells with an electric-voltage gradient. The gradient is established by using electrodes that pass current through the tissue. Within the implant device itself, electrical current is carried by the electrons. However, within tissue or saline, this current is carried by the movement of charged ions such as  $\text{Na}^+$ ,  $\text{Cl}^-$ , and  $\text{H}_2\text{PO}_4^-$ . Devoid of dissolved salt, pure deionized water exhibits a very low conductance. The function of the electrode is to convert the charge transfer between electrons in the circuits to ions in the tissue. It does so through two main mechanisms: a capacitive double-layer charging/discharging and Faradaic processes. Conceptually, this is represented by a circuit with two conduction pathways. Faradaic pathway is a complex impedance that can have both reversible (pseudo-capacitive) and irreversible (conductive) properties (Fig. 1).

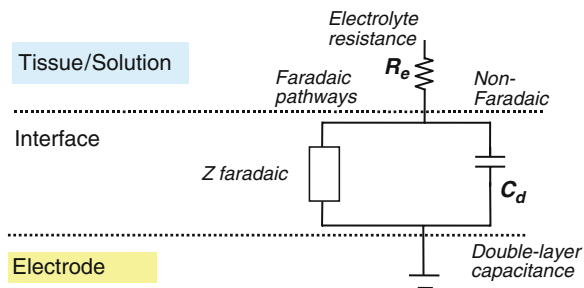


**Fig. 1** Schematic showing the two main charge-injection pathways of the electrode interface

## 2.2 Electrical Double Layer

An electrical double layer is formed whenever a metal is submerged in a liquid. The charges on the metal can attract positive or negative ions, resulting in an ion concentration at the interface region that differs from that in the bulk solution. When a submerged metal is charged, the charges in the metal and oppositely charged ions in the liquid attract each other and concentrate near the electrode-liquid interface. The small separation distance (about 20 nm) between charges in the electrode and in the electrolyte results in high capacitance, typically around 400 nF/mm<sup>2</sup>. The electric double-layer charging is fast acting and carries the majority of the current immediately after the start of a neural stimulation pulse. The double-layer capacitance is not constant, but increases with higher electrode potentials or higher ion concentration levels. This is due to the increased amount of ions that attract to and accumulate at the electrode surface [2].

## 2.3 Reversible Metal Oxidation/Reduction

Traditionally, all the noncapacitive charge-injection mechanisms are grouped together into the “Faradaic” pathway. This includes both the reversible and irreversible chemical reactions. They are grouped together because the distinction between the two can be unclear in some instances. The reversible oxidation/reduction reaction plays an important role for charge injection and it is part of what gives each metal its unique electrochemical properties.

By changing the electrode potential, the metal can be made to react with the surrounding water molecules and ionic species. A common reaction is the formation of metal oxide. When a metal is deprived of electrons (i.e., positively biased), it starts to attract negatively charged ions. With sufficient driving force (in the form of electrical bias), the metal may react with oxygen in water molecules to form an oxide. On the other hand, when a platinum group metal is supplied with abundance of electrons, it can bind to hydrogen atoms to form a reduced hydride form.

The electrical bias at which a particular oxidation-reduction reaction occurs is expressed as the standard potential ( $E^\circ$ ) of a reaction. This standard potential is measured in relation to the voltage at which hydrogen is oxidized ( $\text{H}_2 \rightarrow 2\text{H}^+ + 2\text{e}^-$ ) in acid with 1 M activity. In actual experiments, the reaction voltage is typically measured by comparing the value to a reference electrode (e.g., Ag/AgCl). For example, the Ag/AgCl electrode has a constant potential of 0.2 V when compared to the standard hydrogen electrode (SHE). The voltage measured with AgCl can then be subtracted by 0.2 V to arrive at the standard potential  $E^\circ$  of the reaction. The measured reaction voltage is dependent on the composition of the surrounding electrolyte. For platinum submerged in 1 M sulfuric acid, the reaction voltage for hydrogen gas formation is at 0 V. However, in physiological saline (pH 7), the  $\text{H}_2$  gas formation occurs at  $-0.83$  V.

In saline, platinum oxidation starts at a standard potential  $E^\circ > 0.2$  V. The oxidation reaction can be reversed by negatively biasing the electrode (Fig. 2) (Table 1). At a given voltage,  $E$ , the ratio of oxidized [O] to reduced [R] species can be described by Nernst equation:

$$E = E^0 + \frac{RT}{nF} \ln \frac{[O]}{[R]} \text{ or } \frac{[O]}{[R]} = e^{\frac{nF}{RT}(E-E^0)}$$

**Fig. 2** Equilibrium concentration of oxidized vs. reduced species as function of voltage

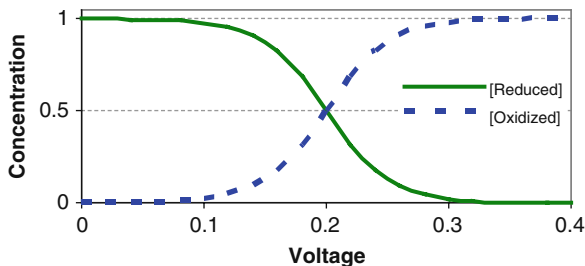


**Table 1** Constants for Nernst equation

---

|   |
|---|
| $R = 8.3 \text{ J/K}\cdot\text{mol}$            |
| $T = 298 \text{ }^\circ\text{K}$                |
| $F = 9.65 \times 10^4 \text{ C/mol}$            |
| $R \cdot T / F = 0.0257 \text{ V}$              |
| $n = \text{number of } e^- \text{ transferred}$ |
| $E = \text{electrode voltage}$                  |

---

### 2.4 Irreversible Chemical Reaction

If the electrode potential is further increased near the electrolysis potential, it will eventually start to decompose water to form oxygen or hydrogen gas. The gas quickly diffuses away, making the reaction chemically irreversible. The irreversible reaction pathway is then dominated by the electrolysis reaction.

In simplified electrode models, the irreversible reaction pathway is typically represented by a resistor  $R_i$ . The resistor denotes that charge is consumed and not stored. However, the pathway actually behaves more like a diode. The reaction-current equation is described approximately by:

$$i = i_0(e^{(V_E - V_{act}) \cdot \frac{n \cdot F}{RT}}),$$

When the electrode voltage ( $V_E$ ) exceeds the reaction potential ( $V_{act}$ ), the current increases exponentially with voltage.

Even at voltages below that of water electrolysis, other undesirable reactions can occur [3]. Two common examples are dissolution of metals by formation of metal chloride and formation of hydrogen peroxide.

While these reactions are typically irreversible, a small portion of them may be reversed in the neuro-stimulation setting. This is because neuro-stimulation typically uses short pulses that are charge balanced. When the current polarity is reversed, the  $H_2$  and  $O_2$  gases still adsorbed on the electrode surface may be dissociated [4]. Likewise, dissolved metal chloride can be electroplated back onto the metal surface.

## 2.5 Electrolyte Resistance

The resistance of an electrolyte, or the tissue surrounding the electrode, is represented by a simple resistor  $R_e$ . In saline, ions can move freely, resulting in low  $R_e$  value of around  $50 \Omega \cdot \text{cm}$ . For a  $10\text{-mm}^2$  electrode implanted in biological tissue, the resistance is typically around  $500\sim 1500 \Omega$ . Certain tissues (e.g., muscle fascia) can also have a small capacitive component, making the impedance slightly frequency dependent. It should be noted that while all the other electrode capacitance and resistance parameters scale with an  $r^2$  relationship, the electrolyte resistance is inversely proportional to the electrode radius  $r$ . The resistance relationship for a hemispherical electrode can be derived by integrating the electrolyte resistance of a hemispherical volume from the electrode surface to infinity. Each slice of the hemispherical shell has an area of  $2 \cdot \pi \cdot r^2$ , and a thickness  $dr$ .

$$R_s = \int \frac{\rho}{A} dl = \int_r^\infty \frac{\rho}{2\pi \cdot r^2} dr = \frac{\rho}{2\pi \cdot r}$$

With increasing distance from the electrode surface, the resistance decreases by  $r^2$ . Therefore, the  $R_s$  is dominated by the solution resistance at the surface of the electrode. For a planar disk electrode,  $R_s = \rho/4r$  [5].

## 3 Common Electrochemical Tests and Electrode Materials

### 3.1 Cyclic Voltammetry

The occurrence of oxidation and electrolysis reactions can be best observed with the slow cyclic voltammetry technique. In this analysis, the electrode voltage is slowly ramped up or down (typically at  $<0.1 \text{ V/s}$ ), and the measured current is plotted in relationship to the voltage (Fig. 3). The slow voltage ramp allows oxidation/reduction to equilibrate, resulting in more well-defined peaks.

If the measured system is just a simple resistor, the current would be linearly proportional to the voltage, as dictated by  $I = V/R$ . If the system were a pure capacitor, the current would be a constant value ( $I = C \cdot dV/dt$ ) (Fig. 4).

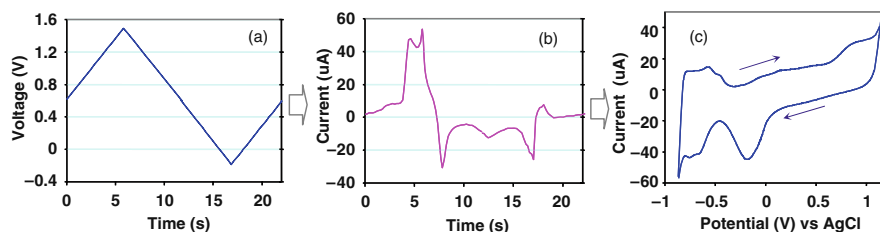
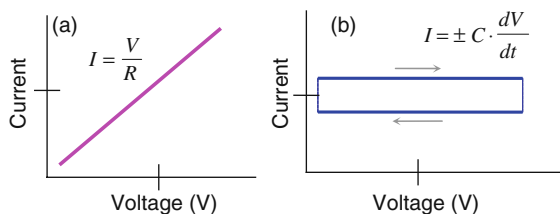


**Fig. 3** In cyclic voltammetry, (a) electrode voltage is ramped up or down, and (b) the current is measured. (c) The result is plotted as current vs. voltage

**Fig. 4** (a) current voltage graph of a simple resistor, and (b) a capacitor



If the electrode surface is oxidized or reduced, there would be a surge of current at the corresponding reaction potential. As seen in Fig. 5, the concentrations of the oxidized and reduced species change near the reaction potential. The resulting current is proportional to the rate of change in the concentration:  $I = d[O]/dt$ .

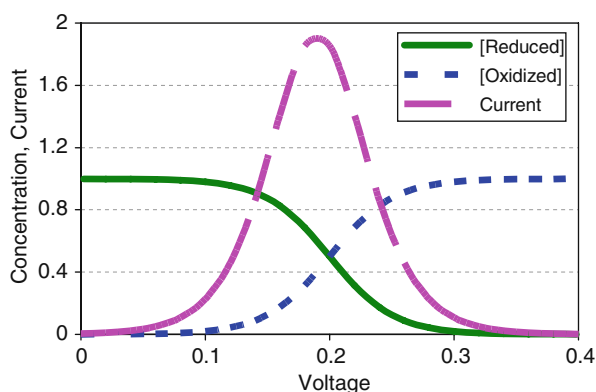


**Fig. 5** The concentration of the reduced vs. oxidized species, and the current as a result of voltage

To obtain a clear CV graph, it is preferable to use electrodes larger than  $3 \text{ mm}^2$ . Using a larger electrode allows for higher levels of oxidation-reduction currents, which can be more clearly recorded over the parasitic capacitance and resistance current levels.

### 3.2 Platinum

The cyclic voltammogram for a smooth, polycrystalline platinum electrode submerged in saline is shown in Fig. 6. The range of the voltage scan is limited by the generation of oxygen gas at  $E^\circ$  of +1.23 V (Fig. 6-1), and hydrogen gas at -0.83 V (Fig. 6-4). This is observed in the curve by the sharp exponential increase in the current when the electrode is near the hydrolysis voltage. The voltage range in which the electrode can be operated without undergoing hydrolysis is referred to as the “water window.”

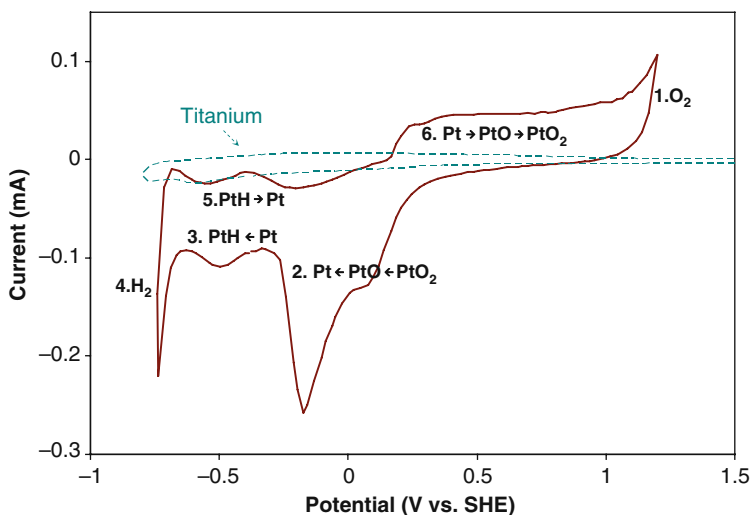


**Fig. 6** Cyclic voltammetry of 4-mm<sup>2</sup> platinum, measured in 0.1-M NaCl in open air (21% oxygen) and a scan rate of 0.1 V/s. The marked points indicate hydrogen released (5), hydrogen plated (3), oxidation of platinum (6), reduction to Pt (2), O<sub>2</sub> generation (1), and H<sub>2</sub> Generation (4)

Within the water window, platinum is observed to undergo several oxidation changes. By removing electrons from platinum (i.e., applying a positive voltage), platinum can be induced to react with oxygen in the water, forming platinum oxide. On the positive sweep, the oxidation reaction starts at 0.2 V (Fig. 6-6) and continues to occur even up to values of 1.23 V. Each platinum atom can be bound to a maximum of 2 oxygen atoms, resulting in a +4 state. Platinum oxide can be made very thick through repeated anodic high-current pulses [6]. On the negative sweep, the oxide is converted back to elemental platinum when the voltage falls below 0.2 V (Fig. 6-2). At more negative voltages, adding excess electrons to platinum can induce hydrogen atoms to bond (Fig. 6-3). Unlike oxygen, hydrogen is only loosely bound to the platinum surface (Table 2).

**Table 2** Platinum reactions, potential listed in reference to standard hydrogen electrode [7]

| Reaction  | $E^\circ$ |
|---|-----------|
| $\text{H}_2(\text{g}) + 2\text{OH}^- \leftrightarrow 2\text{H}_2\text{O} + 2e^-$    | -0.83     |
| $2\text{H}_2\text{O} \leftrightarrow \text{O}_2(\text{g}) + 4\text{H}^+ + 4e^-$     | 1.23      |
| $\text{H}_2\text{O}_2 \leftrightarrow \text{O}_2 + 2\text{H}^+ + 2e^-$              | 0.70      |
| $\text{PtH}_2 + \text{OH}^- \leftrightarrow \text{PtH} + \text{H}_2\text{O} + e^-$  | -0.6      |
| $\text{PtH}_2 + \text{OH}^- \leftrightarrow \text{Pt} + \text{H}_2\text{O} + e^-$   | -0.5      |
| $\text{Pt} + \text{H}_2\text{O} \leftrightarrow \text{PtO} + 2\text{H}^+ + 2e^-$    | 0.25      |
| $\text{PtO} + \text{H}_2\text{O} \leftrightarrow \text{PtO}_2 + 2\text{H}^+ + 2e^-$ | 0.3       |
| $\text{Pt} + 6\text{Cl}^- \leftrightarrow \text{PtCl}_6^{2-}(\text{aq}) + 6e^-$     | 0.73~1.4  |

### 3.3 Titanium

Titanium injects relatively little charge within the operating voltage range. Observation of the reaction potentials shows that only one reversible oxidation reaction occurs within the voltage range, with the oxidation state change between +4 and +3.



With repeated voltage cycling, titanium does not exhibit a charge-injection increase due to “activation” (see iridium). However, the voltage at which oxygen evolution occurs will gradually shift higher. This is due to the buildup of a resistive oxide layer. The increased voltage drop across the oxide requires a higher electrode potential to achieve the hydrolysis current (Fig. 7).

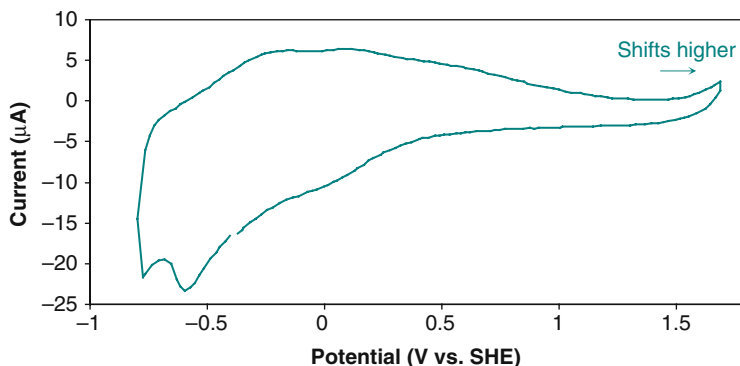


**Fig. 7** Cyclic voltammogram of 4-mm<sup>2</sup> titanium in 0.1 M saline

### 3.4 Iridium

Compared to platinum, iridium can inject an even greater amount of charge through oxidation reactions for the same electrode area, because each individual iridium

**Table 3.** Iridium reactions [11]

|   |  |
|---|--|
| $\text{Ir}^{+3} + 4\text{H}_2\text{O} = \text{IrO}_4^{-2} + 8\text{H}^+ + 3e^-$ | $E^\circ = 1.448 - 0.4576\text{pH} + 0.0197 \log (\text{IrO}_4^{-2}/\text{Ir}^{+3})$ |
| $\text{Ir} + 2\text{H}_2\text{O} = \text{IrO}_2 + 4\text{H}^+ + 4e^-$           | $E^\circ = 0.926 - 0.0391\text{pH}$  |
| $\text{IrO}_2 + 2\text{H}_2\text{O} = \text{IrO}_4^{-2} + 4\text{H}^+ + 2e^-$   | $E^\circ = 2.037 - 0.01182\text{pH} + 0.0293 \log(\text{IrO}_4^{-2})$                |

atom can be bound to a maximum of 4 oxygen atoms to +8 state (Table 3). The iridium surface can also be “activated” with repeated voltage cycling in saline [8–10]. This “activation” process creates a thick layer of porous iridium oxide that further enhances charge injection. Because the activated iridium utilizes the three-dimensional bulk material instead of just the surface, the resulting effective surface area is many times that of the topological area. Cyclic voltammetry analysis shows that for the as-deposited state, the iridium surface can deliver about the same amount of charge as platinum. However, after 400 cycles, the iridium delivers almost 10 times the charge within the same voltage range. Because of the many reaction potentials, the individual current peaks cannot be easily distinguished in the graph (Fig. 8).

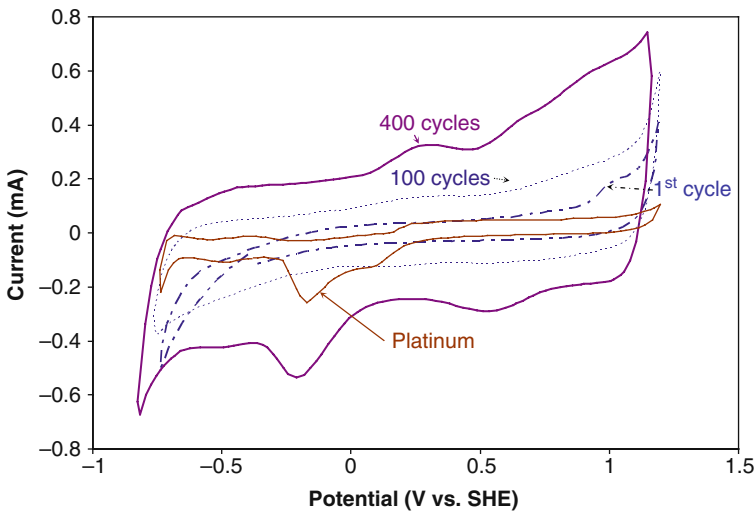


**Fig. 8** Cyclic voltammogram for 4-mm<sup>2</sup> iridium electrode in saline. Current increase is observed with prolonged voltage cycling

By integrating the area within the C-V graph, the iridium charge injection is calculated to be 30 mC/cm<sup>2</sup> [12]. However, not all of this charge is available during neural stimulation. Because of the many oxidation-state changes, iridium charge injection requires many milliseconds to equilibrate. This is the result of slow mass transport of oxygen into the bulk of iridium material. While typical slow cyclic voltammetry takes 1 minute for a complete sweep, neural stimulation

pulses are much shorter, typically less than 1 ms. For the short pulses used in neural stimulation, the practical charge-injection limit for iridium is  $1 \text{ mC/cm}^2$ .

### 3.5 *Effect of Protein*

Protein is known to reduce corrosion for platinum-stimulation electrodes [13]. Studies performed with a quartz-crystal microbalance further show that protein can competitively bind to the platinum surface and prevent oxidation. This study is performed by depositing platinum on a piece of piezo crystal with a natural harmonic frequency of 10 MHz [14]. Voltage cycling the platinum in liquid causes the platinum to oxidize. The additional oxygen mass lowers the harmonic frequency. Each type of amino acid reduces the increased mass by a varying degree. The proteins cause the C-V curve to lose the distinct peaks for platinum and, instead, to show peaks corresponding to the oxidation of the different amino acids.

### 3.6 *Impedance Measurement*

An impedance measurement can be used as a standardized test for quickly estimating the roughness and porosity of a surface. It is performed by applying a small ac voltage signal (10 mV) at various frequencies (typically 10 kHz–0.1 Hz) and using the measured electrode current to calculate its impedance [15–16]. The small-signal perturbation used in the impedance minimizes the oxidation and hydrolysis reactions. The electrode impedance is thus dominated by the double-layer capacitance  $C_d$ , which is in series with the electrolyte resistance  $R_e$ . This forms a high-pass filter with cutoff frequency at:

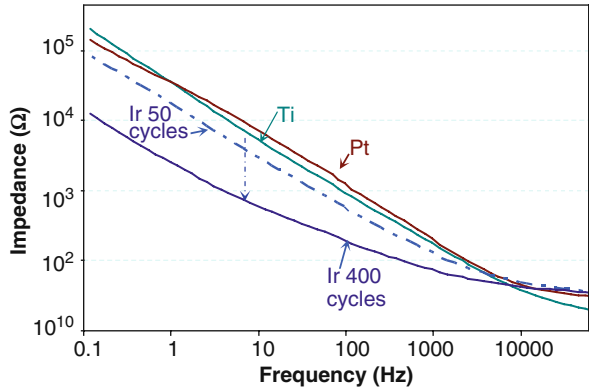
$$f = \frac{1}{2 \cdot \pi \cdot R_e \cdot C_d}$$

At very high frequencies (>10 kHz), the capacitor  $C_d$  shunts all the current, and the resulting electrode impedance is approximately the electrolyte resistance  $R_e$ . At very low frequencies ( $\sim 0.1$  Hz),  $C_d$  becomes an open circuit, resulting in a total electrode impedance of  $R_e + R_i$ . At intermediate frequencies, the impedance is governed by the capacitance:

$$Z = \frac{1}{j \cdot \omega \cdot C}, \text{ with } C \propto A$$

Therefore, an electrode with a rougher surface would exhibit a larger surface area, and thus a higher capacitance. As seen in Fig. 9, three similarly sized electrodes made of titanium, platinum, and iridium exhibit similar impedance values when they are initially submerged. However, after the iridium electrode is subjected to repeated voltage cycles at the full voltage range of the water window (as in cyclic voltammetry), its impedance at lower frequencies decreases by up to 10 fold [17].

**Fig. 9** Impedance spectroscopy of titanium, platinum, and iridium electrodes; all are around 2.5 mm<sup>2</sup> in size. Smaller electrodes are used here so the electrode impedances are above that for connection wires



## 4 Neural Stimulation Settings Which Affect Charge Injections

### 4.1 Basis of Neural Stimulation

Figure 10 depicts an electrode injecting current into the surrounding tissue, with the target neuron nearby. Current passing through the semipermeable cell membrane establishes a voltage gradient across the membrane. If the transmembrane voltage increases by a value that exceeds a threshold (typically 15 mV above the

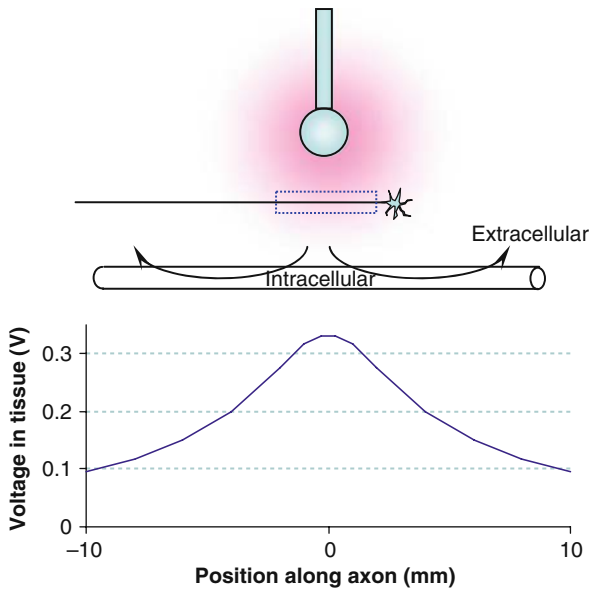


**Fig. 10** An electrode placed near the target neuron, establishing a voltage gradient in tissue

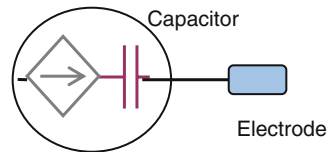
resting state), the voltage change activates a cascade of ion channels that leads to cell excitation.

Neural excitation can be best achieved with an electric field that is nonhomogeneous (i.e., near the edge of an electrode). Calculations using a conducting-cable model show that stimulation efficacy is proportional to the gradient of the electric field along the neural membrane (alternatively this can be calculated as the second spatial derivative of the electric potential) [18]. The nonhomogeneous field increases the current flux into the cell membrane at the region of the highest potential. Current then travels down the axon and exits at regions of the membrane nearby.

## 4.2 Components of a Neural Stimulation System

In order to provide the stimulation pulses to the electrode, the stimulation system typically contains custom circuitry, communication modules, and a power supply (battery). These components are housed in hermetic casing, traditionally made of titanium (Fig. 11).

**Fig. 11** Schematic showing output capacitor



To guarantee safety, a capacitor is placed at the output terminal of the electronics. In the event of electronics failure, in which the output is shorted to one of the supply voltages, the output capacitor is crucial in preventing a continuous DC charge injection. The output capacitor is also useful in implementing charge balance, as can be seen in the monophasic stimulation example (Section 4.3).

## 4.3 Monophasic Voltage Stimulation

Monophasic voltage stimulation is the most basic neuro-stimulation scheme. During stimulation, the circuit outputs a constant-voltage pulse (Fig. 12a). Current is injected through the output capacitor and to the electrode to stimulate the tissue. The current level is limited by the tissue resistance. After the pulse, the circuit output returns to ground. The voltage stored across the output capacitor and electrode interface drives the reaction in reverse and helps to recover the charge.

## 4.4 Constant Voltage vs. Constant Current

Voltage-controlled systems rely on the tissue resistance to limit the current. Due to the buildup of voltage across the capacitor and electrode interface, the remaining voltage drop across the tissue decreases over the pulse duration. This is reflected in

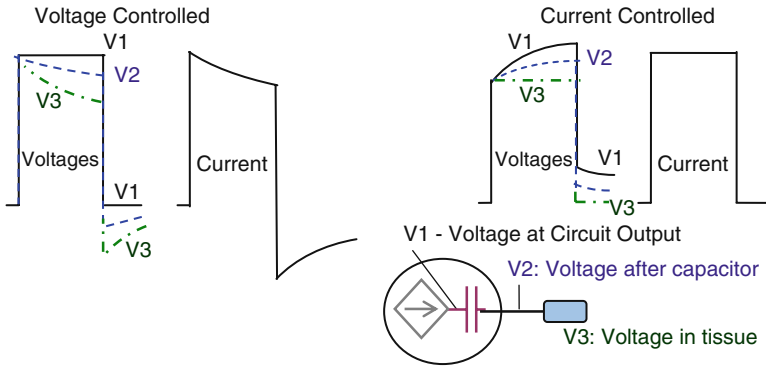


**Fig. 12** Voltage control vs. current control

a nonuniform current level. For certain applications, the initial current spike may actually stimulate other neuron populations that respond to shorter pulses.

The current-controlled scheme avoids this problem by automatically increasing the output voltage to maintain constant current (Fig. 12b). Another benefit for using current control is the ability to use multiple electrodes to establish a constructive current profile. Multiple electrodes cannot be easily implemented with voltage control because the impedance between electrodes can vary depending on the relative distance, leading to uncertainty in the current. The drawback of current control is the increased complexity in the circuit design. Additionally, the p and n type output transistors need to be calibrated to improve charge balance.

#### 4.5 Analysis of Constant-Current Electrode-Voltage Waveform

A diagram of the electrode-voltage waveforms for constant-current stimulation is illustrated in Fig. 13. A constant-current pulse is injected via the counter electrode, and returned through the test electrode (connected to ground). With the onset of constant-current injection, current passing through the electrolyte (or tissue) resistance ( $R_{\Omega}$ ) would result in a voltage drop (Fig. 13a). For some high-current stimulation applications, this resistive voltage drop can exceed 10 V. Because the current level is constant for the pulse duration, the  $iR$  voltage drop also stays constant and can easily be subtracted from the measured voltage. The resistive voltage is not part of the electrode potential because it occurs in the tissue, and is therefore independent of the reactions on the electrode surface. The injected current also charges the double-layer capacitance ( $C_d$ ), resulting in a voltage ramp (Fig. 13b). As the electrode voltage increases, metal oxidation/reduction or other electrode reactions may start to occur. Current injection then becomes divided between the double-layer charging and Faradiac reactions including metal oxidation, thus decreasing the voltage-ramping speed (Fig. 13c). Because metal oxidation stores charge reversibly like a capacitor, it is sometimes termed as ‘pseudo-capacitance.’ If there is a

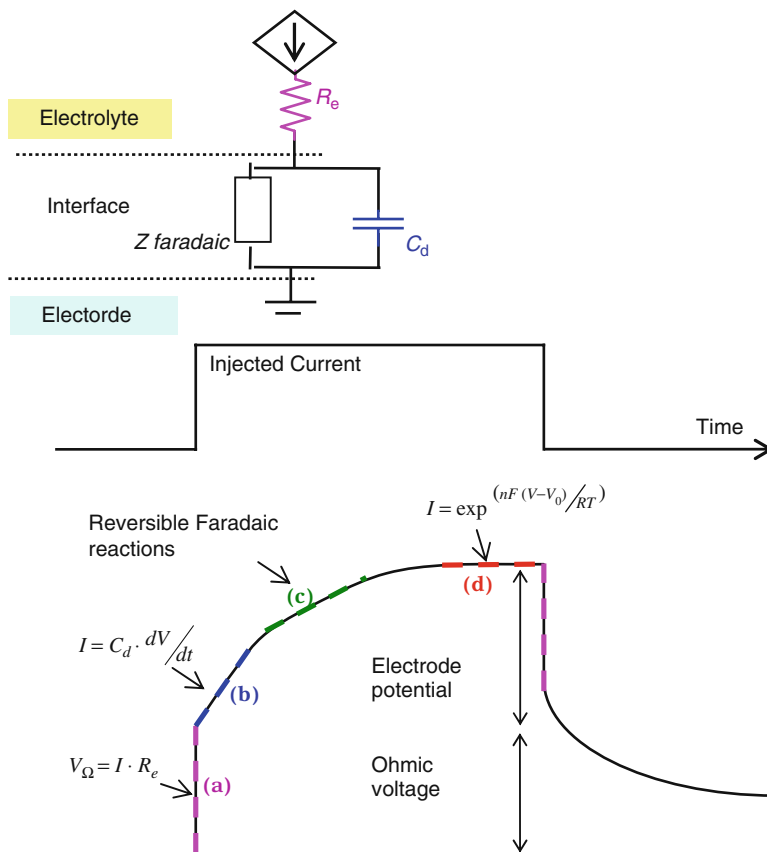


**Fig. 13** Voltage waveform generated by a constant-current pulse through the electrode-electrolyte interface

sufficient increase in electrode potential ( $\sim 1$  V), electrolysis occurs and thus shunts the majority of the current (Fig. 13d). If the electrode is continuously operated in the electrolysis regime, undesirable byproducts are formed and corrosion accelerates [19]. Since the electrode current becomes an exponential function of the voltage when in the electrolysis-dominated regime, a small increase in voltage can cause a large increase in current. This characteristic can be used to identify the onset of hydrolysis.

#### 4.6 Current Control with Passive Recharge

A commonly used neuro-stimulation scheme is to inject charge with a constant-current pulse, then recover the charge by clamping the circuit output back to ground voltage. In the passive recharge phase, the circuit operates similarly to the recharge

phase in the monophasic mode, relying on the voltage stored in the capacitor and electrode to drive the recharge. Passive recharge conserves energy because it utilizes the voltage potential already stored in the capacitor to drive the recharge current. However, it suffers from slower recharge, with some high-current stimulation applications taking more than 10 ms to recover. Due to the limited driving strength of the return pulse, the change in oxidation state may not be completely reversed. Furthermore, leakage current in the output capacitor accumulates over time and as a result the anode typically exhibits signs of corrosion due to the passive recharge (Fig. 14).

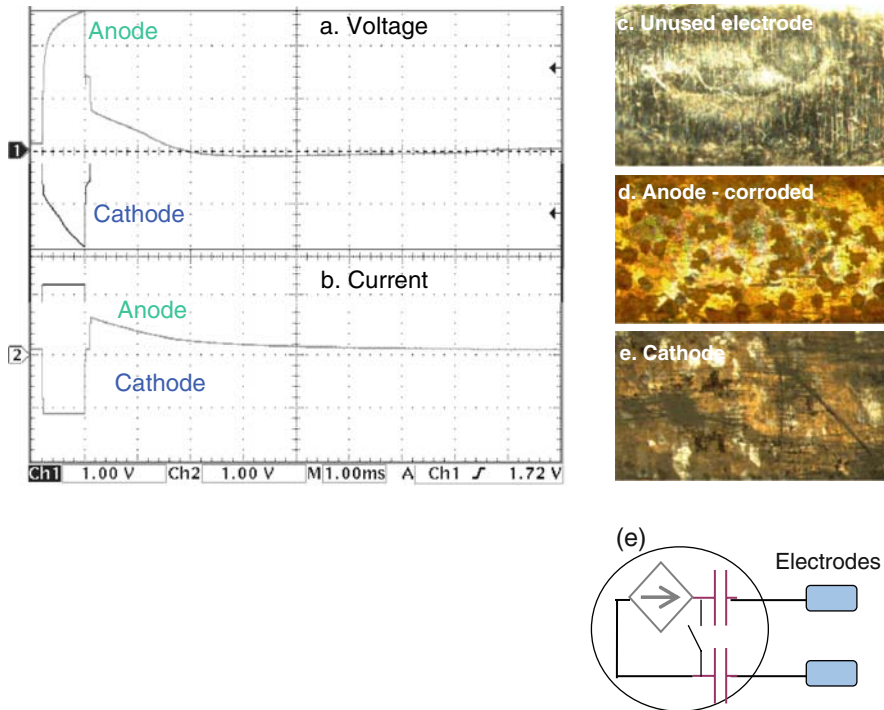


**Fig. 14** Passive recharge observed in the electrode (a) voltage and (b) current waveforms, the resulting corrosion morphology (b–d), and (e) schematic of constant-current injection with passive discharge shorting

### 4.7 Active Recharge

For high-frequency stimulation, active recharge can be used to accelerate the recharge speed. A circuit designed to provide active recharge would actively drive both the cathodic and anodic phases. However, at the end of both active phases, the circuit still needs to incorporate a “shorting” phase, as done in passive recharge.

The shorting phase discharges any residual charge between the two active phases and prevents the bias voltage located at the electronics output (before capacitor) from slowly drifting away from ground.

It is important to note that active recharge may not reduce the likelihood of electrode corrosion. During the recharge phase, the cathode is positively biased and tends to maintain the positive bias at the end of the stimulation sequence, leaving the electrode susceptible to corrosion.

#### ***4.8 Cathodic Bias***

For platinum electrodes, corrosion can be best minimized with a slight cathodic bias, rather than completely balancing the charge [20]. This is because the platinum electrode is more susceptible to corrosion when positively biased, increasing the likelihood for oxidation and dissolution by chloride.

To implement a cathodic bias, a slightly higher amount of charge is injected in the cathodic pulse than the anodic pulse. This ensures that the oxidation that occurs during stimulation can be completely reversed, rather than continuing to build up in successively thicker oxide layers. Since the cathodic bias scheme requires charge imbalance, the output capacitor cannot be used. The imbalance in charge injection must be supplied by a third, sacrificial anode, which is needed to provide sufficient material for corrosion to occur over the device lifetime. While this is technically feasible, the concept of intentionally not balancing charge has not gained wide usage.

#### ***4.9 Bipolar vs. Monopolar Stimulation***

Many devices are designed to operate in either bipolar or monopolar modes, allowing the user to select the most-effective mode.

In bipolar mode, current is passed between two electrodes that are close to each other, resulting in a current pathway that is concentrated between the two electrodes. This leads to localized stimulation in the tissue immediately surrounding the electrodes.

In applications where the target tissue may be located further away or protected by the high-impedance of the dura, monopolar stimulation can be used to increase the stimulation distance. By using a return electrode that is near the implant casing, one creates an electrical gradient that has increased spatial coverage (Fig. 15).

### **5 Other Measurement Techniques**

Cyclic voltammetry and impedance analysis were previously introduced as standard methods for studying the electrochemical properties of the electrode materials. However, these techniques cannot accurately predict the electrode behaviors when

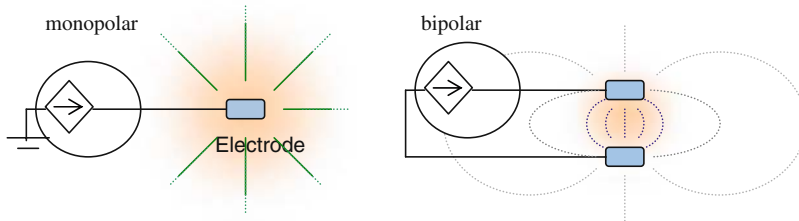


**Fig. 15** Monopolar and bipolar electrode configurations

used in neuro-stimulation applications. Tests that are appropriate for this unique environment are introduced in the following sections. The charge-injection limit of an electrode can be quickly estimated by measuring electrode potential as a function of charge injection. Implementing a pulse-clamp is a new technique that has the potential for measuring the charge-storage characteristics. Finally, computational methods can be used to reveal detailed information describing the charge-injection mechanism.

### 5.1 Electrode-Potential Measurement

A quick method to estimate the safe charge-injection limit of the electrode is to measure the electrode potential as a function of the injected charge [21]. At low charge-injection levels, the electrode potential increases linearly with increasing charge injection as the double-layer capacitance charges. However, with the onset of electrolysis, any additional charge is consumed by hydrolysis and the electrode potential reaches a plateau.

The test is typically conducted by setting a stimulation protocol with a constant pulse width. The current amplitude is then gradually increased as successive measurements are recorded. This sequence is used to avoid the effect of electrode activation. To minimize electrode dissolution, a cathodic pulse measurement of the same magnitude and duration should be made following each anodic pulse measurement.

As shown in Fig. 16, the platinum electrode potential reaches a broad maximum at a current injection of about  $0.15 \text{ mC/cm}^2$ . At greater charge-injection values, the electrode potential appears to gradually decrease. This is likely due to the fact that the electrode experiences surface cleaning and roughening over the duration of the experiment.

Compared to platinum, iridium exhibits a much higher charge-injection limit at about  $0.8 \text{ mC/cm}^2$ . The iridium curve displays a very gradual flattening of the slope. This indicates that with increased charge injection and electrode potential, iridium reaches a greater oxidation state and increased charge-injection effectiveness.

An electrode with a fresh titanium surface shows similar curvature to that of a platinum electrode at low charge densities. However, at charge densities greater than  $0.1 \text{ mC/cm}^2$ , the electrode voltage continues to increase and does not plateau due

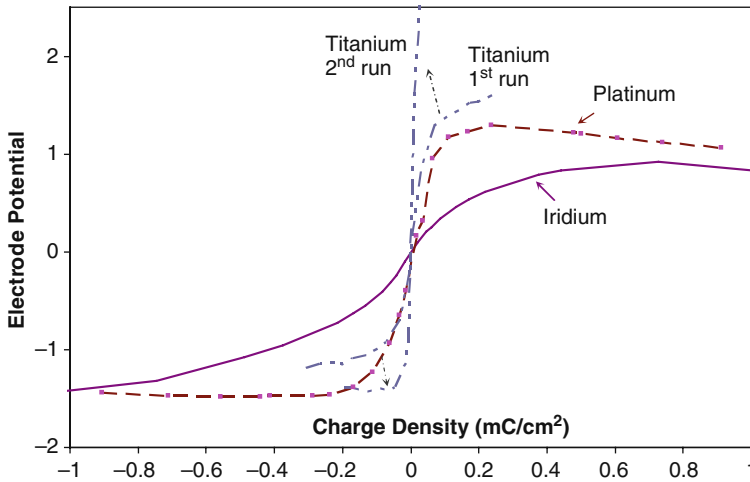


**Fig. 16** Electrode potential for a titanium, platinum, and iridium electrode, measured at the end of 1-ms-long pulse. Titanium measurement is repeated to show drastic increase in electrode potential

to the increased thickness of the resistive oxide layer. When the titanium is immediately tested a second time, the electrode voltage is substantially higher due to the thick oxide layer. The diode-like property of the titanium oxide results in an asymmetrical curvature [22]. For cathodic charging, the curve plateaus at  $-0.05 \text{ mC/cm}^2$ . For the anodic pulsing, the electrode potential continues to increase past 4 V.

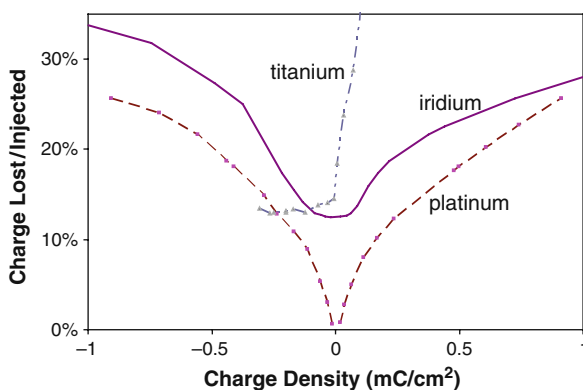
## 5.2 Pulse Clamp

Pulse clamping is a relatively new technique that promises to provide more information about the charge-storage characteristics of neural stimulation electrodes. Pulse-clamp circuits operate similarly to a typical neural stimulation system. The difference lies in the additional circuit components that precisely measure the current level and use positive feedback to greatly accelerate the discharge [23, 24]. A typical pulse-clamp sequence starts with the working electrode set to 0 V (or any voltage) against the counter electrode or the reference electrode in most cases. During testing, the instrument switches to current mode and injects the working electrode with a constant-current cathodic or anodic pulse. Then, the instrument clamps the test electrode potential back to the initial voltage. In this state, all of the charge stored on the working electrode is discharged and detected by the instrument. The charge that is not recovered due to Faradaic loss can thus be calculated. If the electrode behaves as a pure resistor, then no stored charge will be recovered. Conversely, if the electrode behaves as an ideal capacitor, then all of the injected charge will be recovered and measured. The recovered current will exhibit an exponential time decay, with a time constant of  $\tau = R_e \cdot C_d$ , where  $R_e$  is the ohmic electrolyte resistance and  $C_d$  is the electrode capacitance.

When using pulse clamping to compare electrodes of different materials, the difference in discharge time can affect the measurement results. For example, iridium discharges more slowly than platinum, leading to higher measured charge loss. Similarly, larger electrodes also discharge slower because they exhibit greater double-layer capacitance. To facilitate comparison, the discharge time can be reduced by increasing the positive feedback for the slower electrode.

The pulse-clamp result can be displayed as the fraction of charge lost divided by the charge injected (in the constant-current pulse) (Fig. 17). At very low charge density, platinum electrodes behave like ideal capacitors. Utilizing only double-layer capacitance, the stored charge is quickly and completely removed during the discharge phase. With increased charge injection, oxidation-reduction reactions begin to occur. The oxidation reaction is typically not completely reversed during discharging. This is observed in the curve as higher fraction not recovered.

**Fig. 17** Pulse-clamp data of titanium, platinum, and iridium electrodes



Accurately measuring iridium electrodes can be difficult because iridium utilizes bulk oxide with slow reaction kinetics, meaning the discharge time can be greater than 30 ms. Depending on the data-acquisition method, part of the discharge current may be truncated resulting in high level of measured charge loss.

Titanium discharges very quickly, relying almost completely on double-layer charge injection. Unlike platinum or iridium, titanium does not exhibit symmetrical behavior for cathodic and anodic pulses. As a result, the anodic charge injection is almost completely consumed in the formation of oxide. Repeating the experiment produces nearly identical results, despite the fact that the electrode potential has increased.

### 5.3 Computer Simulation

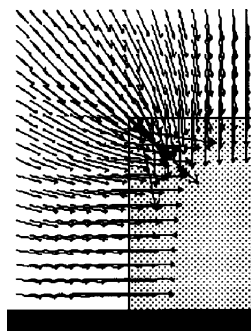
A well-designed model of the electrode interface can greatly stream-line the process of designing new systems and help visualize the reaction dynamics. However, creating a realistic model of the interface is difficult, due to its complex nonlinear behavior. If one were to create a detailed model that can simulate cyclic voltammetry,

one would need a set of equivalent elements for each individual reaction that occurs at different potentials [25–27]. For example, according to Table 2, modeling platinum would require at least 7 equivalent pathways, with each pathway containing information about the reaction speed, potential, and charge capacity. However, it is possible to use a much simplified model if one just needs an accurate computer representation for a particular stimulation condition.

Because neuro-stimulation occurs at a relatively fast time scale, the reactions do not have time to equilibrate. To simulate the condition of many reactions occurring concurrently, one just needs the average impedance during the entire pulse duration. Typically, good simulation can be obtained using a second-order model similar to Fig. 1. The drawback is that because the electrode behavior is dependent on the stimulation conditions, this model may lose accuracy when applied to different pulse width and amplitude settings.

Computer simulations have long been used to reflect a reactive electrode surface, such as when a high charge injection results in high level of electrolysis current [28–31]. These simulations employ a resistive network, and all illustrate significant increases in current density at convex protrusions (Fig. 18).

**Fig. 18** Resistive models reflect the current-crowding pattern that occurs in hydrolysis regime or with DC bias [30]

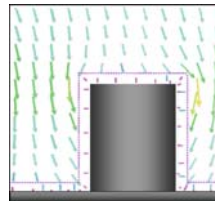


In normal usage, electrodes should avoid reaching electrolysis potentials [32], and instead rely on the double-layer capacitance and reversible oxidation/reduction mechanisms. To simulate the electrode behavior in this regime, capacitive elements are needed. Because the voltage of the capacitive elements is the result of charge accumulation over time, a time-stepping computation is necessary to track the behavior of these capacitive elements through the pulse duration. SPICE and ANSYS are shown as two examples of software that can be used to perform this time-stepping simulation. The parameters are obtained from curve-fitting SPICE simulation to recorded pulse-clamp data, using 1-ms pulse width and charge density of  $0.1 \text{ mC/cm}^2$  [33].

Performing the time-domain simulation with ANSYS illustrates the typical current pathway that for capacitive electrode surfaces (Fig. 19). Areas of higher current are observed in the solution near the sharp convex edges. However, at the electrode-resolution interface, the current density is low and uniform. This is shown in the short arrows near the electrode surface that are perpendicular to the surface. The increased

current density in the solution is the result of current having to navigate around the protruding portions of the electrode. Compared to the resistive model, the capacitive electrode model shows a very different current pattern. This uniform current distribution on the electrode surface is reflected in dissolution testing in Section 5.4.

**Fig. 19** ANSYS-simulation of a nonflat electrode operated in capacitive regime, 50  $\mu\text{s}$  after the start of current injection. Vectors indicate the direction and magnitude of current



The same simulation can be performed using SPICE to illustrate the current contribution from different pathways. Because SPICE lacks meshing capability, a custom C-script is required to generate a netlist of nodes that describe the two-dimensional space of the electrode surface and surrounding electrolyte. Figure 19 shows the simulated current densities for the protruding and recessed portions of the electrode. At the beginning of the pulse, there is a brief 20- $\mu\text{s}$  duration in which higher current concentrates on the convex protrusions (Fig. 20a). This initial current spike is required to charge the capacitance and establish proper voltage bias. The voltage gradient is established after 20  $\mu\text{s}$ , and the current density becomes uniform, with less than 2% variation on the entire electrode surface.

As the electrode voltage increases during the pulse, a proportionally higher amount of current is injected through the metal-oxidation pathway, rising to more

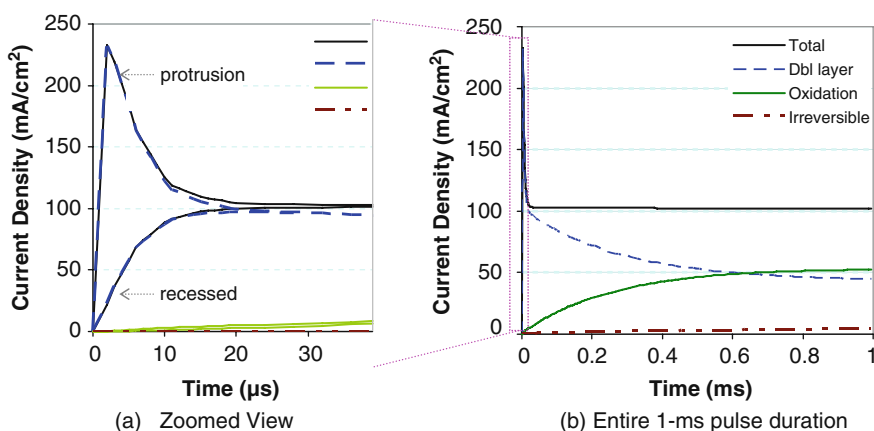


**Fig. 20** Contribution of charge injection from different mechanisms. The expanded view in (a) shows the first 50  $\mu\text{s}$

than 50% at the end of the 1-ms pulse. The electrolysis current remains low, contributing less than 5% of the total current at 1 ms.

### 5.4 Dissolution Testing

Dissolution testing can be performed to illustrate the current distribution at different charge-injection settings. To demonstrate the effect of extreme surface topology, gold microposts (10- $\mu\text{m}$  wide and tall) are electroplated on top of a gold electrode surface [34]. Gold is used in this test because it dissolves readily during the anodic pulse and is redeposited on the metal surface during the cathodic pulse. The deposition pattern is a good indication of the current distribution.

The morphology of surface redeposition shows a pattern of uniform current density when the electrode is injected with  $30\ \mu\text{C}/\text{cm}^2$ , well within its charge-injection limit. However, at  $2\ \text{mC}/\text{cm}^2$ , increased current density is observed at sharp convex edges, indicating a dissolution-dominated mode of charge injection at the higher current level (Fig. 21).

In general, long-term dissolution testing is required to ensure the lifetime of an electrode. The various techniques introduced in this chapter are useful in estimating the electrode performance at different usage conditions, but they cannot be substituted for the dissolution test. The test is generally conducted with the electrode submerged in buffered saline, with oxygen purged from the saline. The stimulation is set to the maximum pulse width and current amplitude used in clinical setting. The frequency may be further increased to speed up the experiment.

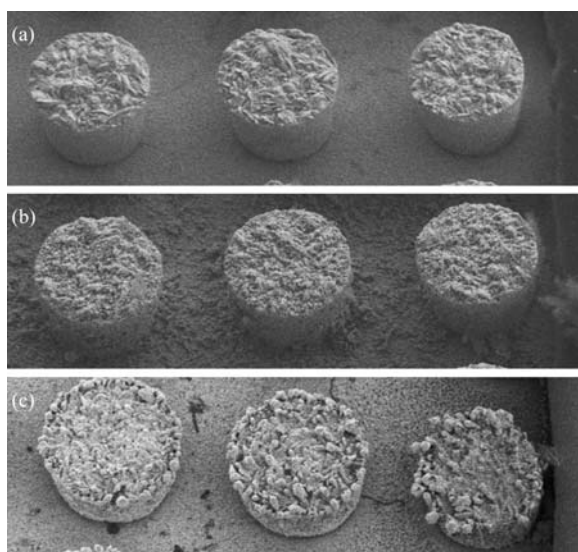


**Fig. 21** SEM image of an array of gold microposts (a) as fabricated, (b) subjected to  $30\ \mu\text{C}/\text{cm}^2$  dissolution for 2 weeks and (c)  $2\ \text{mC}/\text{cm}^2$  dissolution

## 5.5 Inductively Coupled Plasma (ICP)

The most effective method of measuring the dissolved ion is with ICP equipment. The test solution containing dissolved metal is nebulized into the chamber. A radio-frequency field generates plasma and the optical spectrum of the plasma is analyzed for emission from various elements.

Most ICP equipments are not optimized for analyzing samples with high carbon contents. If protein is added to the test solution, it may quickly leave a carbon deposit on the optics. For these samples, one should instead use inductively coupled plasma-mass spectrometry (ICP-MS). An ICP-MS ionizes the sample in the plasma chamber and then uses mass spectrometry to detect the different elements. While ICP has sensitivity of parts-per-billion range, ICP-MS can detect in the parts-per-trillion range.

## 6 Summary

This chapter introduced several methods for analyzing the electrochemical properties of neuro-stimulation electrodes. Cyclic voltammetry is a generic technique that shows the oxidation/reduction potentials of a material, thereby revealing important electrode behavior properties. Furthermore, the impedance spectra and the electrode potential can reflect the surface area and the charge-injection limit of the electrode, respectively. Lastly, to determine their functional lifetimes, electrodes must be subjected to long-term dissolution testing.

The computer simulations described in this chapter are very simplistic models, with parameters obtained by fitting to actual stimulation waveforms. This type of simulation can only reflect the electrode behavior within a narrow range of charge-injection settings. Nevertheless, with better understanding of the materials, future models might be able to predict the electrode behavior at all charge-injection conditions, and even predict the rate of corrosion.

## References

1. Rose TL, Kelliher EM, Robblee LS (1985) Assessment of capacitor electrodes for intracortical neural stimulation. *J Neurosci Meth* 12 (3):181–193
2. Bard AJ, Faulkner LR (1980) *Electrochemical methods: fundamentals and applications*. John Wiley & Sons, New York
3. Brummer SB, McHardy J, Turner MJ (1977) Electrical stimulation with Pt electrodes: trace analysis for dissolved platinum and other dissolved electrochemical products. *Brain Behav Evol* 14:10–22
4. Morton SI, Daroux MI, Mortimer JT (1994) The role of oxygen reduction in electrical stimulation of neural tissue. *J Electrochem Soc* 141:122
5. Newman J (1966) Resistance for flow of current to a disk. *J Electrochem Soc* 113:501
6. Tremiliosi-Filho G, Jerkiewicz G, Conway BE (1992) Characterization and significance of the sequence of stages of oxide film formation at platinum generated by strong anodic polarization. *Langmuir* 8:658

7. Pikelny AY (2003) Mechanism of platinum deterioration under stimulation pulses polarization. *IFESS*
8. Petit MA, Plichon V (1997) Anodic electrodeposition of iridium oxide films. *J Electroanal Chem* 444:247–252
9. Weiland JD, Anderson DJ, Humayun MS (2002) In vitro electrical properties for iridium oxide versus titanium nitride stimulating electrodes. *IEEE Trans Biomed Eng* 49:1574–1579
10. Wessling B, Besmehn A, Mokwa W et al. (2007) Reactively sputtered iridium oxide. *J electroch Soc* 154:f83–f89
11. Pourbaix M (1974) *Atlas of electrochemical equilibria in aqueous solutions*. Pergamon Press, Brussels
12. Beebe X, Rose TL (1988) Charge injection limits of activated iridium oxide electrodes with 0.2 ms pulses in bicarbonate buffered saline. *IEEE Trans Biomed Eng* 35:6
13. Robblee LS, McHardy J, Marston JM, Brummer SB (1980) Electrical stimulation with Pt electrodes V The effect of protein on Pt dissolution. *Biomaterials* 1(3):135–139
14. Hibbert DB, Weitzner K, Tabor B, Carter P (2000) Mass changes and dissolution of platinum during electrical stimulation in artificial perilymph solution. *Biomaterials* 21(1): 2177–2182
15. Macdonald JR (1992) Impedance spectroscopy. *J Annals Biomed Eng* 20:289–305
16. Norlin A, Pan J, Leygraf C (2005) Investigation of electrochemical behavior of stimulation/sensing materials for pacemaker electrode applications I Pt, Ti, and TiN coated electrodes. *J Electrochem Soc* 152 (2):J7–J15
17. Meyer RD, Cogan SE, Nguyen TH et al. (2001) Electrodeposited iridium oxide for neural stimulation and recording electrodes. *IEEE Trans Neural Sys Rehab* 9:2
18. Durand DM (1999) Electrical stimulation of excitable tissue. *Biomedical Engineering Handbook*. CRC, Boca Raton, FL
19. Robblee LS, McHardy J, Agnew WF et al. (1983) Electrical stimulation with Pt electrodes VII, Dissolution of Pt electrodes during electrical stimulation of the cat cerebral cortex. *J Neurosci Methods* 9(4):301–308
20. Scheiner A, Mortimer JT, Roessmann U (1990) Imbalanced biphasic electrical stimulation: muscle tissue damage. *Ann Biomed Eng* 18(4): 407–425
21. Rose TL, Robblee LS (1990) Electrical stimulation with Pt electrodes VIII Electrochemically safe charge injection limits with 0.2 ms pulses. *IEEE T BioMed Eng* 37:1118
22. Campbell SA, Kim HS, Gilmer DC et al. (1999) Titanium dioxide (TiO<sub>2</sub>)-based gate insulators. *IBM J Res Dev* 43(3):383–392
23. Bonner M, Daroux M, Crish T et al. (1993) The pulse-clamp method for analyzing the electrochemistry on neural stimulating electrodes. *J Electrochem Soc* 140:2740
24. Hung A, Zhou D, Greenberg R et al. (2007) Pulse-clamp technique for characterizing neural-stimulating electrodes. *J Electrochem Soc* 154(9):479–486
25. Moorhead ED, Stephens MM (1990) A finite element Galerkin/B-spline (GBS) numerical model of electrochemical kinetics, transport, and mechanism for multi-geometry working electrodes II: A study of quasi-reversible linear sweep voltammetry. *J Electroanal Chem* 282(1):1–26
26. Speiser B (1996) Numerical simulation of electroanalytical experiments: recent advances in methodology. *Electroanal Chem* 19:1–108
27. Alden J (1998) *Computational electrochemistry*, PhD Thesis, Oxford University, <http://compton.chem.ox.ac.uk/john/Thesis/>
28. Feldberg SW (1972) *Electrochemistry, calculations, simulations and instrumentations*. Marcel Dekker, New York
29. Goldberg IB, Bard AJ (1972) Resistive effects in thin electrochemical cells: digital simulations of current and potential steps in thin layer electrochemical cells. *Electroanal Chem* 38:313
30. Ferrigno R, Brevet PF, Girault HH (1997) Finite element simulation of the chrono-ampereometric response of recessed and protruding microdisc electrodes. *Electrochimica Acta* 42(12):1895–1903

31. McIntyre CC, Grill WM (2001) Finite element analysis of the current-density and electric field generated by metal microelectrodes. *Ann Biomed Eng* 29(3):227–235
32. Rubinstein JT, Spelman FA, Soma M (1987) Current-density profiles of surface mounted and recessed electrodes for neural prostheses. *IEEE Trans Biomed Eng* 34 (11):864–875
33. Ksienski DA (1992) A minimum profile uniform current-density electrode. *IEEE Trans BioMed Eng* 39(7):682
34. Brummer SB, Turner MJ (1977) Electrical stimulation with Pt electrodes: II-estimation of maximum surface redox limits. *IEEE Trans BioMed Eng* 24:440
35. Hung A (2005) Techniques for sensing the current distribution and charge storage of high-density neuroelectrodes. PhD Thesis UCLA
36. Hung A, Zhou D, Greenberg R et al. (2005) Dynamic simulation and testing of the electrode-electrolyte interface of 3-D stimulating microelectrodes. *IEEE Neural Eng*, March 16–19